Titre: Title:	Macro-scale numerical investigation of the contribution of Van der Waals force to the pressure-drop overshoot in fine-particle fluidized beds
Auteurs: Authors:	Youssef Badran, Renaud Ansart, Jamal Chaouki, & Olivier Simonin
Date:	2024
Type:	Article de revue / Article
Référence: Citation:	Badran, Y., Ansart, R., Chaouki, J., & Simonin, O. (2024). Macro-scale numerical investigation of the contribution of Van der Waals force to the pressure-drop overshoot in fine-particle fluidized beds. Powder Technology, 436, 119505 (9 pages). https://doi.org/10.1016/j.powtec.2024.119505

|	
URL de PolyPublie: PolyPublie URL:	https://publications.polymtl.ca/57573/
Version:	Version officielle de l'éditeur / Published version Révisé par les pairs / Refereed
Conditions d'utilisation: Terms of Use:	CC BY-NC-ND

Document publié chez l'éditeur officiel
Document issued by the official publisher

Titre de la revue: Journal Title:	Powder Technology (vol. 436)
Maison d'édition: Publisher:	Elsevier
URL officiel: Official URL:	https://doi.org/10.1016/j.powtec.2024.119505
Mention légale: Legal notice:	© 2024 The Authors. Published by Elsevier B.V. This is an open access article under the CC BY-NC-ND license (http://creativecommons.org/licenses/bync-nd/4.0/).
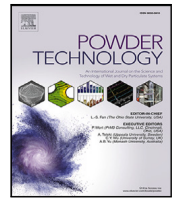
Macro-scale numerical investigation of the contribution of Van der Waals force to the pressure-drop overshoot in fine-particle fluidized beds

Youssef Badran [a,b], Renaud Ansart [a], Jamal Chaouki [b], Olivier Simonin [c,*]

[a] Laboratoire de Génie Chimique, Université de Toulouse, CNRS, INPT, UPS, Toulouse, France
[b] Department of Chemical Engineering, Polytechnique Montréal, P.O. Box 6079, Station Centre-ville, Montréal, Québec H3C 3A7, Canada
[c] Institut de Mécanique des Fluides de Toulouse (IMFT), Université de Toulouse, CNRS, Toulouse, France

HIGHLIGHTS

- Two adhesion pressure closures are given for the Van der Waals force effect in TFM.
- The kinetic theory fails to predict a pressure overshoot in a fluidized bed.
- The coordination number model is successful in generating the pressure overshoot.
- Interparticle Van der Waals force contributes to the pressure overshoot phenomenon.

GRAPHICAL ABSTRACT
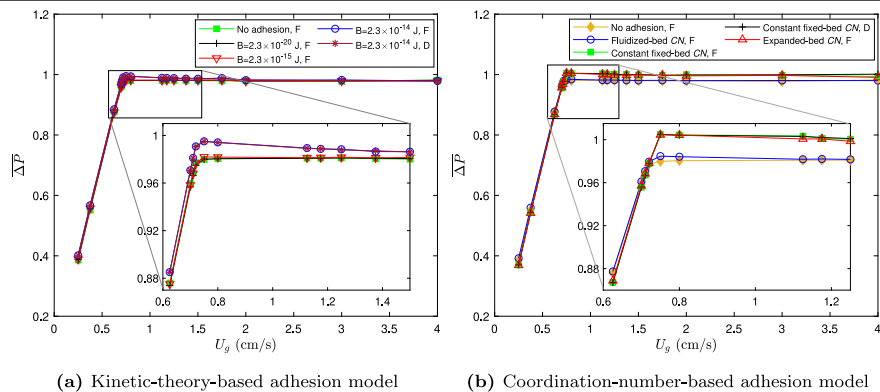
(a) Kinetic-theory-based adhesion model   (b) Coordination-number-based adhesion model

ARTICLE INFO

ABSTRACT

Interparticle Van der Waals force contributes to the overshoot in the bed pressure drop at the minimum fluidization velocity during the transition from static to fluidized bed conditions, which is a well-known phenomenon in the fluidization of fine particles. In this study, two adhesive particle pressure closures considering the effect of interparticle Van der Waals force are used in two-fluid model simulations with the intention to generate the pressure overshoot. The first adhesive pressure model developed within the context of the kinetic theory of rapid granular flows failed to produce the overshoot due to the dominance of multiple and long duration contacts in the fixed-bed flow. Another closure based on the coordination number was then proposed to represent long-lasting interparticle contacts, which gave an adhesive contribution much larger than the one of the kinetic theory model and was able to create the pressure drop overshoot.

1. Introduction

Gas–solid fluidized beds are employed in several industries, such as the polymerization of olefins, fluid catalytic cracking (FCC), coal combustion, and ore roasting [1]. Good quality solids mixing, high rates of mass and heat transfer, uniform temperature distribution, and the capability of processing a broad variety of granular materials are among the features of fluidized-bed reactors [1–5]. Interparticle forces, such as Van der Waals, electrostatic, liquid bridge, and solid bridge forces, may have a significant influence on fluidized bed hydrodynamics and performance [6–12].

Fine particles ranging from cohesive to aeratable are highly desirable for reactive fluidization processes due to their high surface-to-volume ratio, which results in greater reaction rates per unit volume of reactor [13]. The pressure drop overshoot at the minimum fluidization velocity is a typically encountered phenomenon in beds of fine particles belonging to the group A of Geldart's classification [14]. A more intense overshoot and a larger hysteresis area between the fluidization and defluidization pressure-drop curves are observed upon decreasing the particle diameter towards Geldart's C group [15]. This observation is owing to the dominant role of interparticle over hydrodynamic interactions in static beds of these particles. The Van der Waals adhesive force is the dominating interaction force between fine particles in a dry ambient environment [16].

Van der Waals forces include dipole–dipole, dipole-induced dipole, and instantaneous dipole-induced dipole forces acting between atoms and molecules. The temporal average of a neutral atom's dipole moment is zero, yet at every instant there is a definite polar moment provided by the asymmetrical electron distribution around the protons that are inside the nucleus [17]. This instantaneous dipole produces an electric field, which creates a dipole moment in any adjacent neutral atom [17]. The two dipoles then interact, resulting in a force of attraction among the two atoms. The temporal average of this instantaneous dipole-induced dipole force, which is also known as the London dispersion force, is finite. Hamaker [18] obtained an expression for the Van der Waals force between macroscopic objects using the dispersion interaction potential between two atoms/molecules proposed by London [19] and an additivity hypothesis (summing up the forces over all pairs of individual atoms/molecules). The Van der Waals force between particles in contact is highly influenced by their surface roughness (i.e., asperity size) [20,21].

Working at high temperatures and/or high pressures has an impact on the strength of Van der Waals force. The Van der Waals force increases with temperature due to greater molecular dipole pulsation and a larger particle–particle contact area induced by viscoelastic flattening [21–24]. The magnitude of the Van der Waals force can rise with pressure owing to gas adsorption on the particle surfaces [4,25,26]. It is worth mentioning that hydrodynamic forces can increase dramatically with pressure (gas density increases with pressure), which may result in a less prominent influence of interparticle interactions on the bed hydrodynamics [4].

Stresses caused by adhesive and frictional interactions have a significant influence on the mechanical response of granular media [27]. There is, however, insufficient data on the magnitude of these stresses, which limits comprehension of the fluidization behavior reported in experimental studies. Mutsers and Rietema [28] and Tsinontides and Jackson [29] postulated that the interparticle contact adhesion and friction are responsible for the stable expansion occurring between the minimum fluidization and minimum bubbling velocities in fine-particle beds. Rietema and Piepers [30] ascribed the pressure drop overshoot at incipient fluidization to interparticle and particle–wall forces. According to these authors, the Van der Waals interaction is the source of particle–particle force. The non-sphericity can enhance the solid friction and the pressure-drop hysteresis [31–34].

In the experiments carried out by Vanni et al. [32], the static wall friction effect on the pressure overshoot was only noticeable in columns with small diameters ($D = 2$ cm). The experiments of Srivastava and Sundaresan [27] also revealed a more significant overshoot in smaller columns, which they ascribed to particle–wall friction. Wang et al. [35] observed that increasing the static bed height increases the pressure overshoot intensity, which they attributed to wall friction. The effect of bed diameter and height on the significance of static wall friction (bridging) can also be seen in the vertical solid stress profiles showing the Janssen effect in silos and hoppers [36,37].

Several researchers accounted for the Van der Waals force in the Eulerian–Lagrangian model to simulate the fluidization behavior of fine particles. Ho and Sommerfeld [38] used a criterion for agglomeration based on a critical velocity determined from an energy conservation between before and after collision that takes into account the Van der Waals force. These authors considered that when the normal relative velocity between two interacting particles is smaller than the critical velocity, agglomeration occurs. Wang et al. [39] solved a Newtonian equation of motion with a Van der Waals force term based on the Hamaker theory for each particle in a fluidized bed riser. Zhang et al. [40] investigated the cluster dynamics in circulating fluidized-bed reactors using a CFD-DEM model. Their simulations showed that when the solid volume fraction α_p is large, the Van der Waals interaction may promote the cluster formation.

On the other hand, Eulerian–Eulerian models that take into consideration the impact of interparticle Van der Waals interaction are scarce in the literature. Within the framework of the kinetic theory of granular flows, Gidaspow and Huilin [41] added a negative pressure inferred from the experimental data of radial distribution functions to the solid pressure in order to consider the effect of adhesive forces on the fluidization of FCC particles. This empirical adhesive pressure modified the kinetic theory equation of state to match the measured particle pressure. Parmentier [42] worked on incorporating the effect of Van der Waals interaction into the two-fluid model utilizing the BBGKY hierarchy. An adhesive pressure was added to the particle pressure to account for the Van der Waals attraction between particles. By comparing the magnitudes of attractive and repulsive solids pressures within a bed of Geldart A particles in the fluidized state (small attraction), Parmentier [42] concluded that the overestimation of bed expansion found in standard two-fluid model simulations is not due to neglecting the effect of the Van der Waals force. The kinetic theory based on the assumptions of binary collision and molecular chaos may be extended from moderately dense to highly dense gas–solid flows by utilizing numerical data of discrete element simulations [43–45].

Some efforts have been made to predict the pressure-drop overshoot phenomenon observed during the fluidization of fine particles. Srivastava and Sundaresan [27] and Loezos et al. [46] utilized a one-dimensional force balance model based on Janssen's approach in order to predict the pressure drop overshoot. This model involves determining coefficients that can combine the adhesion and friction effects together. For instance, when the particle diameter decreases, the friction coefficient of Loezos et al. [46] increases, which may be attributed to an increase in the significance of the Van der Waals adhesive interaction. Ye et al. [47] demonstrated through discrete particle simulations that the pressure overshoot is caused by particle–particle Van der Waals adhesion and particle–wall friction. Weber and Hrenya [48] conducted discrete particle simulations employing Hamaker and square-well adhesion models. Their findings reveal that the overshoot in the bed pressure drop is dominated by interparticle adhesion. The Hamaker model predicted that Van der Waals adhesive interactions with the sidewalls have a considerable impact on the pressure-drop overshoot (adhesion augments wall friction), whereas adhesive interactions with the distributor plate have minimal impact. The square-well model, on the other hand, predicted that particle-distributor plate adhesion has a considerable influence on the pressure-drop overshoot.

Interparticle adhesive forces affect both solid pressure and viscosity (normal and shear stresses) [49–51]. The influence of particle viscosity on the pressure overshoot, which is associated with a fixed arrangement of particles (zero particle velocity), is negligible. Hence, we consider only the effect of adhesion on the solid pressure. In our investigation, we take into account the short-range Van der Waals interaction between particles via an adhesive pressure gradient in the particle momentum equation within an Eulerian–Eulerian approach. We present two adhesive pressure models, one based on the kinetic theory and another based on the coordination number to represent interparticle contacts, and assess their capability of creating a pressure-drop overshoot in beds of Geldart A particles.
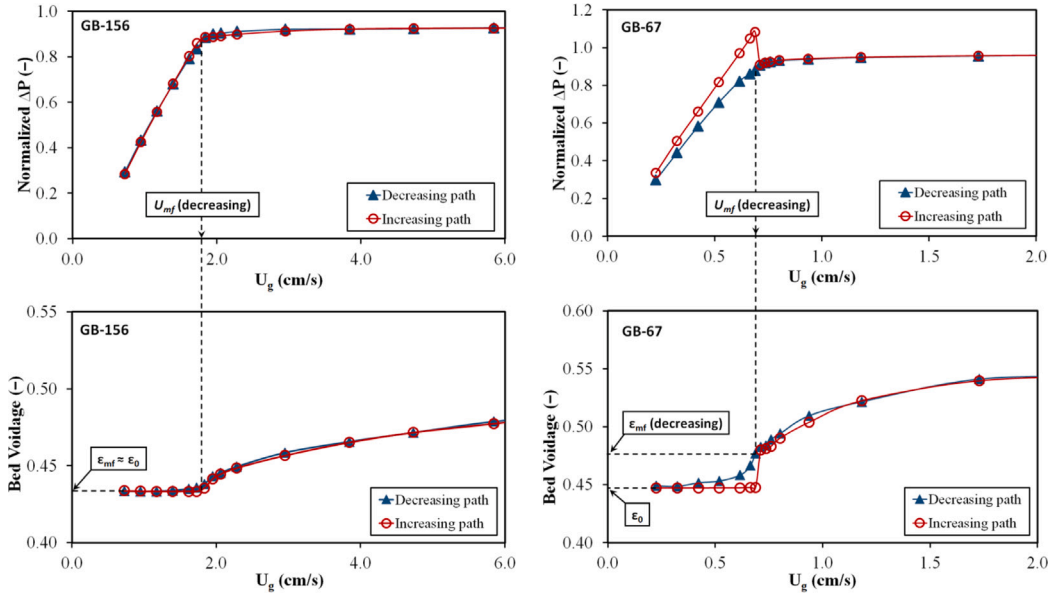
Fig. 1. Normalized bed pressure drop and corresponding voidage profiles of Geldart B (GB-156) and A (GB-67) particles measured by Soleimani et al. [14].

Table 1
Properties of particles used in the experiments of Soleimani et al. [14].

Material	Glass beads	Glass beads
Mean particle diameter, d_p (μm)	156	67
Particle density, ρ_p (kg/m³)	2595	2595
Sphericity	~ 1	~ 1
Geldart group	B	A
Acronym	GB-156	GB-67

2. Prediction of overshoot in pressure drop across an aeratable-particle bed

Soleimani et al. [14] performed experimental measurements of the total bed pressure drop and bed voidage of Geldart A and Geldart B particles fluidized by air at 20 °C. The air was pre-dried by passing it through a bed of humidity adsorber. As a result, capillary forces have a negligible effect. The properties of the solids used in their study are shown in Table 1. The experiments were carried out in a fluidized bed of 5.25 cm in diameter and 50 cm in height. The static bed height was around 15 cm. For details about the procedure employed to determine the experimental bed pressure drop and voidage, the reader is referred to the paper of Soleimani et al. [14].

The experimental bed pressure drop and voidage profiles as a function of the superficial gas velocity of the Geldart B and A glass beads determined by Soleimani et al. [14] are demonstrated in Fig. 1. It can be seen that the increasing velocity path pressure drop curve of the Geldart B particles has no overshoot since the associated loose-fixed-bed and minimum fluidization voidages (ε_0 and ε_{mf}, respectively) are nearly equal. In contrast, a considerable pressure drop overshoot is apparent at the minimum fluidization velocity (U_{mf}) in the fluidization branch of the experiment with Geldart A particles, which is equivalent to the difference between the fixed-bed and minimum fluidization voidages.

In our study, we perform two-fluid simulations using the neptune_cfd code [52]. Transport equations and models employed in this code are reported in Ansart et al. [53]. The particle stress in the Eulerian–Eulerian model consists of kinetic, collisional and frictional terms. The closure of the kinetic and collisional stresses is based on the kinetic theory of granular flows. In dilute flows $(\alpha_p < 1\%)$, the kinetic stress is dominant, whereas in moderately dense flows $(\alpha_p > 5\%)$, the collisional stress dominates. The particle friction stress is employed at high solid volume fractions to take into account the interaction of single

particles with several neighbors through prolonged contact. The normal particle–particle forces are considered via the particle pressure [54]. For the particle frictional pressure, we have employed the following semi-empirical model proposed by Johnson and Jackson [55,56]:

$$P_p^f = \begin{cases} Fr \dfrac{(\alpha_p - \alpha_{p,min})^n}{(\alpha_{p,max} - \alpha_p)^m} & \text{for } \alpha_p > \alpha_{p,min} \\ 0 & \text{for } \alpha_p \leq \alpha_{p,min} \end{cases} \tag{1}$$

where Fr, n and m are constants and $\alpha_{p,min}$ and $\alpha_{p,max}$ are respectively the threshold particle volume fraction for the activation of the frictional stress and the close-packing particle volume fraction. The values of these parameters used in our simulations are listed in Table 2. To account for the Van der Waals interaction among particles, a negative adhesive pressure is added to the particle pressure for all values of the particle volume fraction α_p in our work. The additional negative stress component has the effect of lowering particle repulsion. In the following sections, we propose two adhesive pressure models and investigate their ability to create a pressure drop overshoot.

2.1. Derivation of an adhesive pressure model based on the kinetic theory

The kinetic theory approach relies on the similarity between the random particle movement in rapid granular flow and the thermal motion of molecules in gas [57]. The adhesive pressure model derivation employing the kinetic theory of granular flows given in this subsection is based on the research of Parmentier [42]. Using the BBGKY hierarchy, the Van der Waals force can be included in the Boltzmann–Liouville equation:

$$\frac{\partial f_p}{\partial t} + \frac{\partial}{\partial x_i}\left(c_{p,i} f_p\right) + \frac{\partial}{\partial c_{p,i}}\left(\left\langle \frac{F_{p,i}}{m_p} \mid \mathbf{x_p} = \mathbf{x}, \mathbf{u_p} = \mathbf{c_p}\right\rangle f_p\right)$$
$$= \left(\frac{\partial f_p}{\partial t}\right)_{coll} + \left(\frac{\partial f_p}{\partial t}\right)_{ad} \tag{2}$$

with [58]

$$\left(\frac{\partial f_p}{\partial t}\right)_{ad} = \iint \frac{\partial f_p^{(2)}}{\partial c_{p,i}} \frac{\partial}{\partial x_i}\left(\frac{V(\|\mathbf{x}^* - \mathbf{x}\|)}{m_p}\right) d\mathbf{c_p^*} d\mathbf{x}^* \tag{3}$$

where f_p is the one-particle probability density function defined such that $f_p(\mathbf{c_p}, \mathbf{x}, t)\, \delta\mathbf{c_p}\delta\mathbf{x}$ is the probable number of particles, whose center of mass, $\mathbf{x_p}$, at time t is located in the volume $[\mathbf{x}, \mathbf{x} + \delta\mathbf{x}]$ with a velocity

$\mathbf{u_p}$ in $[\mathbf{c_p}, \mathbf{c_p}+\delta\mathbf{c_p}]$. $F_{p,i}$ represents the external forces acting on the particles (gravity, drag and buoyancy). $F_{p,i}/m_p = du_{p,i}/dt$ is the acceleration of a particle. $\langle F_{p,i} \mid \mathbf{x_p} = \mathbf{x}, \mathbf{u_p} = \mathbf{c_p} \rangle$ represents the conditional average of the external force acting on a particle at a given center position $\mathbf{x_p} = \mathbf{x}$ with the translation velocity $\mathbf{u_p} = \mathbf{c_p}$. The two terms on the right-hand side of Eq. (2) denote the rate of change in the probability density function caused by particle–particle collision and Van der Waals adhesion, respectively. The adhesion term is given by Eq. (3), where $f_p^{(2)}\left(\mathbf{c_p}, \mathbf{x}, \mathbf{c_p^*}, \mathbf{x^*}, t\right)$ is the two-particle probability density function and $V\left(\|\mathbf{x^*} - \mathbf{x}\|\right)$ is the interaction potential between two particles resulting in an adhesion force. According to Elimelech et al. [59], the Van der Waals interaction potential between two spheres can be expressed as follows:

$$V\left(\|\mathbf{x^*} - \mathbf{x}\|\right) = -\frac{A}{24}\left[\frac{2}{2u + u^2} + \frac{2}{(1 + u)^2} + 4\ln\left(\frac{2u + u^2}{[1 + u]^2}\right)\right] \tag{4}$$

where $u = \|\mathbf{x^*} - \mathbf{x}\|/d_p - 1$ is the dimensionless distance between the two particle surfaces and A is the Hamaker constant, which relies on the composition of the particles and the interstitial fluid. The adhesive force exerted by particle p^*, with its center at $\mathbf{x^*}$, on particle p, with its center at $\mathbf{x}$, as a result of the Van der Waals potential given by Eq. (4) can be written as:

$$\mathbf{F}_{p^* \to p}^{ad} = \frac{A}{6d_p}\frac{1}{(2u + u^2)^2}\frac{1}{(1 + u)^3}\frac{\mathbf{x^*} - \mathbf{x}}{\|\mathbf{x^*} - \mathbf{x}\|} \tag{5}$$

For distances between the surfaces of two particles less than a typical interatomic distance S_0, Eqs. (4) and (5) are no longer applicable and the magnitude of the Van der Waals force is fixed at a maximal value in order to represent the physical particle–particle repulsion and prevent the single attraction when the surface separation distance is zero [60].

Assuming that the velocities of colliding particles are not correlated (Enskog approximation for dense flows), the two-particle probability density function is defined as follows:

$$f_p^{(2)}\left(\mathbf{c_p}, \mathbf{x}, \mathbf{c_p^*}, \mathbf{x^*}, t\right) = g\left(\mathbf{x}, \mathbf{x^*}\right) f_p\left(\mathbf{c_p}, \mathbf{x}, t\right) f_p\left(\mathbf{c_p^*}, \mathbf{x^*}, t\right) \tag{6}$$

with $g\left(\mathbf{x}, \mathbf{x^*}\right)$ being the two-particle radial distribution function. The adhesion term in Eq. (3) can then be written as:

$$\left(\frac{\partial f_p}{\partial t}\right)_{ad} = -\frac{\partial}{\partial c_{p,i}}\left(\frac{F_{a,i}}{m_p}f_p\right) - \frac{\partial}{\partial c_{p,i}}\left(\frac{F_{b,i}}{m_p}f_p\right) \tag{7}$$

with

$$F_{a,i} = -\frac{\partial}{\partial x_i}\int n_p\left(\mathbf{x^*}\right) g\left(\mathbf{x}, \mathbf{x^*}\right) V\left(\|\mathbf{x^*} - \mathbf{x}\|\right) d\mathbf{x^*} \tag{8}$$

$$F_{b,i} = \int n_p\left(\mathbf{x^*}\right) \frac{\partial g\left(\mathbf{x}, \mathbf{x^*}\right)}{\partial x_i} V\left(\|\mathbf{x^*} - \mathbf{x}\|\right) d\mathbf{x^*} \tag{9}$$

where n_p is the particle number density. $F_{a,i}$ and $F_{b,i}$ can be approximated as follows:

$$F_{a,i} \approx -\frac{\partial}{\partial x_i} n_p\left(\mathbf{x}\right) g_0\left(\mathbf{x}\right) \int V\left(\|\mathbf{x^*} - \mathbf{x}\|\right) d\mathbf{x^*} \tag{10}$$

$$F_{b,i} \approx 0 \tag{11}$$

where g_0 is the radial distribution function at contact. A momentum balance equation for the solid phase containing a gradient of adhesive particle pressure can then be derived from the Boltzmann–Liouville equation (Eq. (2)):

$$\begin{aligned}\alpha_p \rho_p \frac{\partial U_{p,i}}{\partial t} + \alpha_p \rho_p U_{p,j} \frac{\partial U_{p,i}}{\partial x_j} = &-\alpha_p \frac{\partial P_g}{\partial x_i} + \alpha_p \rho_p g_i + I_{g \to p,i} \\ &- \frac{\partial}{\partial x_j}\left(\alpha_p \rho_p R_{p,ij} + \Theta_{p,ij}\right) - \alpha_p \frac{\partial P_{ad}}{\partial x_i}\end{aligned} \tag{12}$$

where $I_{g \to p,i}$ is the mean interphase gas-to-particle momentum transfer and $R_{p,ij}$ and $\Theta_{p,ij}$ are respectively the particle kinetic and collisional stress tensors. Eq. (12) is derived by substituting (7) in (2) and then multiplying (2) by $m_p\mathbf{c_p}$ and integrating over all velocities $\mathbf{c_p}$. In Eq. (12), $-\alpha_p \partial P_{ad}/\partial x_i$ is equal to $n_p F_{a,i}$, where $F_{a,i}$ is expressed

by Eq. (10). P_{ad} represents an adhesive pressure resulting from the attraction between particles, which is given by:

$$P_{ad} \approx \frac{n_p g_0}{\pi d_p^3/6}\int V\left(\|\mathbf{x^*} - \mathbf{x}\|\right) d\mathbf{x^*} \tag{13}$$

In the case of Van der Waals interaction potential, P_{ad} may be written as:

$$P_{ad} \approx \frac{n_p g_0}{\pi d_p^3/6}\int_{\|\mathbf{x^*}-\mathbf{x}\|>d_p+S_0} V\left(\|\mathbf{x^*} - \mathbf{x}\|\right) d\mathbf{x^*} \tag{14}$$

And according to Parmentier [42]:

$$P_{ad} \approx -A n_p g_0 \ln\left(\frac{d_p}{S_0}\right) \tag{15}$$

The adhesion term in the momentum equation (Eq. (12)) is written as:

$$-\alpha_p \frac{\partial P_{ad}}{\partial x_i} = -\frac{\partial P_p^a}{\partial x_i} \tag{16}$$

with

$$P_p^a \approx -A\frac{n_p}{\alpha_p}\ln\left(\frac{d_p}{S_0}\right)\int_0^{\alpha_p} \alpha_p\left(g_0 + \alpha_p\frac{\partial g_0}{\partial \alpha_p}\right) d\alpha_p \tag{17}$$

The radial distribution function, g_0, which may be viewed as a measure for the likelihood of particle–particle collision, is given as the following expression [61]:

$$g_0 = \left(1 - \frac{\alpha_p}{\alpha_{p,max}}\right)^{-2.5\alpha_{p,max}} \tag{18}$$

Using Eq. (17), the negative adhesive pressure can then be formulated as:

$$P_p^a = -\frac{B}{d_p^3}2\alpha_{p,max}^2\left[\frac{25}{6} + \left(-\frac{3}{2}\frac{\alpha_p^2}{\alpha_{p,max}^2} + \frac{20}{3}\frac{\alpha_p}{\alpha_{p,max}} - \frac{25}{6}\right)g_0\right] \tag{19}$$

with

$$B = A\frac{3}{\pi}\ln\left(\frac{d_p}{S_0}\right) \tag{20}$$

where d_p is the particle diameter, α_p is the solid volume fraction, A is the Hamaker constant, and S_0 is a minimum cutoff separation distance between two particle surfaces. The adhesive pressure P_p^a given by Eq. (19) is added to the kinetic, collisional, and frictional pressures.

2.2. Evaluation of the kinetic-theory-based adhesion model

The adhesive pressure model presented in Eq. (19) is tested by adding it to the solids pressure and performing two-fluid model simulations similar to CFD-DEM simulations carried out by Hou et al. [62]. The values of the parameters used in our quasi-two-dimensional fluidized bed simulations of Geldart A particles are summarized in Table 2. The value of the initial solid volume fraction ($\alpha_{p,ini} = 0.6$) is chosen to be the same as that obtained from the CFD-DEM simulations of Hou et al. [62] for the fixed bed. The bottom face of the cuboid bed employed in our simulations acts as an inlet for gas and a wall with a no-slip condition for particles. The top face serves as a free outlet for both gas and solid phases with an imposed gauge pressure of zero. The left and right faces (normal to the x-axis) are walls for both phases with a no-slip condition for each phase. A symmetry boundary condition is employed for both phases at the front and back faces (normal to the y-axis).

The equations for the kinetic, collisional and frictional solids stress closures employed in our simulations can be found in Ansart et al. [53]. The frictional viscosity is omitted from each simulation with adhesion (only the frictional pressure is included) since it turns negative in the region where adhesion effect is dominant over friction effect. The drag model used is that proposed by Gobin et al. [63], which is the drag correlation of Wen and Yu [64] limited by the Ergun [65] equation for dense regimes. The gas flow is assumed to be laminar (no

Table 2
Simulation parameters.

Parameter	Value
Particle diameter, d_p	100 μm
Particle density, ρ_p	1440 kg/m³
Particle–particle normal restitution coefficient, e_c	0.8
Gas density, ρ_g	1.205 kg/m³
Gas viscosity, μ_g	1.8×10^{-5} Pa s
Cuboid bed size, $L_x \times L_y \times L_z$	$60d_p \times 4d_p \times 200d_p$
Cell size, $\Delta x = \Delta y = \Delta z$	$2d_p$
Initial particle bed height, H_{ini}	$36d_p$
Initial particle volume fraction, $\alpha_{p,ini}$	0.6
Frictional pressure constant (Eq. (1)), Fr	0.05 Pa
Frictional pressure constant (Eq. (1)), n	2
Frictional pressure constant (Eq. (1)), m	5
Threshold solid volume fraction for friction, $\alpha_{p,min}$	0.58
Close-packing solid volume fraction, $\alpha_{p,max}$	0.64
Minimum surface separation distance, S_0	1 nm
Base value of the Hamaker constant, A	2.1×10^{-21} J
Maximum Courant number, CFL_{max}	0.1

turbulence model is used). The agitation model used for the solid phase is $q_p^2 - q_{gp}$, which includes transport equations for the particle fluctuant kinetic energy, q_p^2, and the gas-particle velocity covariance, q_{gp} [57,66–68]. However, since the gas flow is assumed to be laminar, the gas fluctuating velocity $u''_{g,i}$ is zero; hence $q_{gp} = \langle u''_{g,i} u''_{p,i} \rangle_p$ equals zero.

Two sidewall pressure monitoring points at zero and $195d_p$ above the inlet were utilized to measure the overall bed pressure drop at each superficial gas velocity in fluidization and defluidization cycles. Each superficial gas velocity was sustained for 5 s, and the pressure was averaged over the last 2 s of each of these 5 s intervals to determine the time-averaged bed pressure drop values:

$$\overline{\Delta P} = \overline{P_1} - \overline{P_2} = \frac{1}{\sum_{k=1}^{N_r} \Delta t_k} \left(\sum_{k=1}^{N_r} \Delta t_k P_{1,k} - \sum_{k=1}^{N_r} \Delta t_k P_{2,k} \right) \quad (21)$$

where P_1 and P_2 are the pressures at the monitoring points, Δt is the time step, and N_r is the total number of time steps in the 2 s interval. The normalized bed pressure drop is defined as the ratio of the pressure drop across the whole bed to the pressure drop equivalent to the weight of the particles, $\overline{\Delta P}/\Delta P_{eq}$. The pressure drop ΔP_{eq} can be expressed as:

$$\Delta P_{eq} = m_b g / S_b = \alpha_p \rho_p H_b g \quad (22)$$

where m_b is the mass of the particles bed, g is the gravitational acceleration, S_b is the cross-sectional area of the bed, and H_b is the bed height. Substituting 0.6 for α_p and $36d_p$ for H_b (see Table 2) in Eq. (22) gives ΔP_{eq} equals 30.513 Pa. The spatial average of the solid volume fraction α_p is computed as follows:

$$\langle \alpha_p \rangle = \frac{1}{N_c} \sum_{i=1}^{N_c} \alpha_{p_i} \quad (23)$$

where N_c is the number of cells between the inlet and $34d_p$ above the inlet, which is slightly less than the bed height at the lowest superficial gas velocity. The time average of the spatially averaged α_p is determined as:

$$\overline{\langle \alpha_p \rangle} = \frac{\sum_{k=1}^{N_r} \Delta t_k \langle \alpha_p \rangle_k}{\sum_{k=1}^{N_r} \Delta t_k} \quad (24)$$

Then, the bed voidage is obtained as: $\overline{\langle \alpha_g \rangle} = 1 - \overline{\langle \alpha_p \rangle}$.

Bed pressure drop and voidage versus superficial gas velocity curves for fluidization and defluidization cycles with different B values (Eq. (19)) are shown in Fig. 2. The value of B obtained by substituting the values of A, d_p and S_0 (given in Table 2) in Eq. (20) is 2.3×10^{-20}

J. In addition to this value, we tested much higher B values in order to demonstrate that the adhesion provided by the kinetic theory model is several orders of magnitude smaller than that given by the coordination number model presented later in Section 2.3. As depicted in Fig. 2, generating a pressure drop overshoot requires multiplying B by 10^6 (using $B = 2.3 \times 10^{-14}$ J) and no hysteretic behavior is predicted between the increasing and decreasing velocity path curves. The bed voidage curves displayed in Fig. 2 show a decrease in the average gas volume fraction in the bed for $B = 2.3 \times 10^{-14}$ J due to the relatively strong adhesion.

Based on the foregoing results, the adhesive contribution introduced by the kinetic theory model is insufficient to generate an overshoot in the bed pressure drop. This inability might be attributed to the binary and instantaneous collisions assumption used in the kinetic theory approach because fixed-bed flows are dominated by the influence of multiple and sustained contacts. The pressure-drop hysteresis between the fluidization and defluidization branches is not produced because the impact of deformation history is not taken into account in the kinetic theory adhesion model. In particular, the adhesive pressure is only a function of the particle volume fraction α_p, indicating that it is a symmetric closure. In the next section, we present a coordination-number-based approach suitable for quasi-static flow regimes.

2.3. Derivation of an adhesive pressure based on the coordination number

Here, we derive an adhesive pressure model by assuming that the dominant Van der Waals interaction occurs between particles in long-lasting contact characterized by the coordination number. The coordination number is defined as the mean number of particles in contact with a given particle, which may be written as:

$$CN = 2 \frac{n_c}{n_p} \quad (25)$$

where n_c denotes the mean number of contacts per unit volume and n_p denotes the number of particles per unit volume. The factor 2 enters in Eq. (25) because each contact is shared by two particles. The particle–particle stress tensor component due to the adhesive force may be computed as [70–72]:

$$\sigma_{ij}^{ad} = -\frac{1}{V} \sum_{c \in V} f_i^c b_j^c \quad (26)$$

where the sum is over all the contact points c in volume V. f_i^c represents the interaction force between two particles in contact at c and b_j^c represents the vector connecting the centers of these two particles if both centers are inside the volume V, or only the part in V if one of the centers is outside V. By using Eq. (5), the adhesive contact force can be expressed as follows:

$$\mathbf{F}_{p^* \to p}^c = \frac{A}{6d_p} \frac{1}{\left(2u_0 + u_0^2\right)^2} \frac{1}{\left(1 + u_0\right)^3} \mathbf{k}^* \approx \frac{A}{6d_p} \frac{1}{4u_0^2} \mathbf{k}^* \quad (27)$$

where $u_0 = S_0/d_p$ is the minimum dimensionless separation distance between two particle surfaces and $\mathbf{k}^* = (\mathbf{x}^* - \mathbf{x})/\|\mathbf{x}^* - \mathbf{x}\|$ is the unit vector along the line of centers of two interacting particles. Substituting Eq. (27) into Eq. (26) gives the following adhesive stress expression for homogeneous systems:

$$\sigma_{ij}^{ad} = \frac{1}{V} \sum_{c \in V} \frac{A}{24u_0^2} k_i^* k_j^* \quad (28)$$

The isotropic component of the adhesive stress given by Eq. (28) is the adhesive pressure:

$$P_p^a = -\frac{\sigma_{ii}^{ad}}{3} = -\frac{n_c}{3} \frac{A d_p^2}{24 S_0^2} \quad (29)$$

Then, using Eqs. (25) and (29), the adhesive particle pressure can be expressed as:

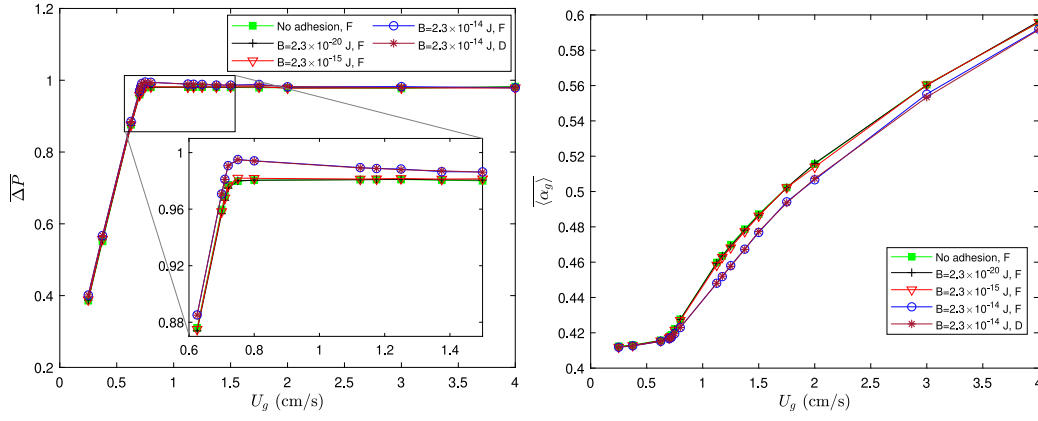$$P_p^a = -\frac{\alpha_p}{\pi d_p^2} CN \frac{A d_p}{24 S_0^2} \quad (30)$$

Fig. 2. Normalized time-averaged overall bed pressure drop and time-spatial averaged gas volume fraction in the bed during fluidization and defluidization cycles with different *B* values in the adhesion pressure (Eq. (19)). *F* represents a fluidization branch and *D* a defluidization branch in this and Fig. 4. [69].

where CN is the coordination number.

2.4. Evaluation of the coordination-number-based adhesion model

Eulerian–Eulerian simulations were carried out using the parameter values in Table 2 to check the ability of the adhesive pressure model given by Eq. (30) to create the pressure drop overshoot. These simulations are the same as those described in Section 2.2, except that the coordination-number-based adhesive pressure model is utilized instead of the kinetic-theory-based one. In our tests, we used a constant coordination number of 4.77 corresponding to a fixed bed state and correlations between the coordination number and the solid volume fraction based on the CFD-DEM simulation results of Hou et al. [62]:

$$CN = 2 + 3.25\alpha_p^{0.4} \qquad \text{for expanded beds} \qquad (31)$$

$$CN = 4.87 \times 10^{-5} \frac{1 - (1 - \alpha_p)^{2.8}}{(1 - \alpha_p)^{11.6}} \qquad \text{for fluidized beds} \qquad (32)$$

These correlations were developed using simulations that account for the Van der Waals adhesion between particles. Fig. 3 shows CN plotted as a function of α_p for expanded and fluidized bed states using Eqs. (31) and (32). In the expanded bed state, as the solid volume fraction decreases from the close-packing value (0.64) to zero, the coordination number slowly decreases until it reaches a minimum value of 2 corresponding to a chain-like structure, as demonstrated in Fig. 3. On the other hand, the coordination number corresponding to the fluidized bed state decreases rapidly towards zero when the solid volume fraction decreases, as seen in Fig. 3. The obtained bed pressure drop and mean gas volume fraction profiles are illustrated in Fig. 4. As we can observe in the pressure drop versus superficial gas velocity plots, the constant fixed-bed coordination number and the expanded-bed correlation both generate overshoot, while the fluidized-bed correlation does not. Based on these results, we can infer that the coordination-number-based model provides an adhesive contribution large enough to produce an overshoot in the bed pressure drop.

The experimental bed voidage curves of Geldart A particles in Fig. 1 demonstrate that at superficial gas velocities less than the minimum fluidization velocity U_{mf}, the bed voidage remains constant at ε_0 in the increasing velocity path. When the superficial gas velocity reaches U_{mf}, the forces exerted by the gas on the particles overcome the interparticle forces, particle–wall friction, and particles' weight, leading to the destruction of the contact network and an abrupt jump in the bed voidage from ε_0 to ε_{mf}. In contrast, in the decreasing velocity path, the bed voidage progressively decreases from ε_{mf} to ε_0 as the superficial gas velocity decreases from U_{mf} to zero. The simulation results in Fig. 4 show a decrease in bed voidage owing to adhesion, but the hysteretic behavior between the fluidization and defluidization cycle curves observed experimentally is not predicted. To obtain this behavior, the role
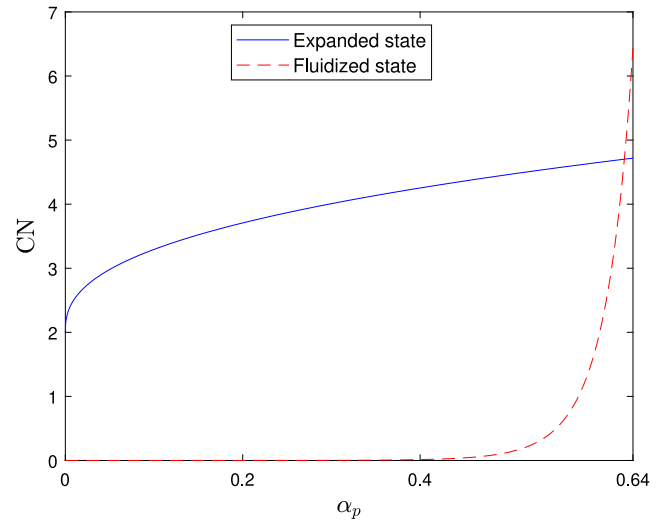

Fig. 3. CN as a function of α_p for expanded and fluidized bed states.

of Van der Waals interparticle force and particle–wall static friction should be dominant over that of hydrodynamic forces in the fixed bed state. Achieving this condition is influenced by the values of the various simulation model parameters. For example, the particle diameter in the experiments of Soleimani et al. [14] is 67 μm, which is smaller than the particle diameter in our simulations (100 μm). In addition, the contact network formation and destruction (the coordination number evolution) should be taken into consideration in our two-fluid simulations to generate the hysteresis. Moreover, the effect of boundary conditions (particle–wall friction) and dimensionality (quasi-2D to 3D) on the pressure overshoot should be explored. Considering the effect of static particle–wall friction on the pressure-drop overshoot in the two-fluid model could be the subject of future research. Accounting for this effect is essential to achieve a quantitative prediction because static wall friction may increase the overshoot intensity. However, the significance of this impact depends on the column diameter [32]. Regarding the effect of particle size, our simulations using the coordination-number-based model demonstrated that the diminution of the particle diameter notably increases the pressure overshoot intensity (data not shown here), which is consistent with experimental observations [15].

The number of interparticle contacts, and hence the radial distribution function, is influenced by adhesion. This could be investigated through DEM simulations. In the fixed-bed state, the dominant effect is for the frictional pressure and not the collisional pressure. Therefore, modifying the radial distribution function to consider the influence of
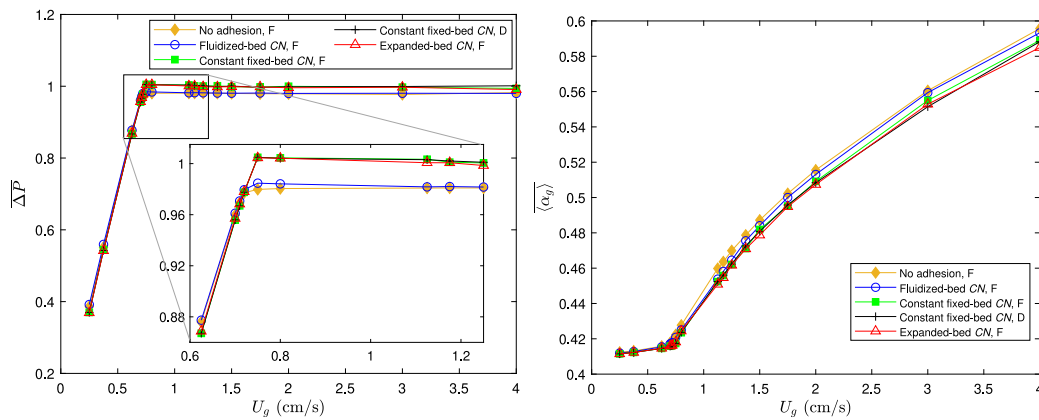
Fig. 4. Normalized time-averaged overall bed pressure drop and time-spatial averaged gas volume fraction in the bed during fluidization and defluidization cycles without and with adhesion using the coordination-number-based model [69].

adhesion may have a negligible effect on the overshoot obtained using the coordination number model. The kinetic theory adhesion model gives an adhesive contribution 6 orders of magnitude smaller than that of the coordination number model. This is because the kinetic theory assumptions, including the assumption that the radial distribution function is not modified by adhesion, are not valid.

3. Conclusion

In this research, two-fluid model simulations were performed with the aim of predicting the pressure-drop overshoot observed during fluidization of Geldart A particles. Two adhesive pressure models were suggested to account for the Van der Waals force among particles. The first model, which is based on the kinetic theory, gives an adhesion effect that is not strong enough to create the pressure drop overshoot. This model may be suitable for rapid granular flows, but it is not appropriate for quasi-static flows because it does not account for the long term and multiple particle–particle contacts. The second model, which is expressed in terms of the mean number of contacts per particle, makes use of CFD-DEM correlations that relate the coordination number to the solid volume fraction for various flow conditions. This model gives an adhesive contribution far larger than the one of the kinetic theory model and produces the overshoot in the bed pressure drop. The success of the aforementioned model appears to be attributable to the fact that it accounts for the multiple and sustained contacts. The hysteresis between the fluidization and defluidization branches was not predicted by any of the two adhesive pressure models.

A meso-scale numerical investigation is required to guide postulating a continuum evolution equation for the coordination number or developing an Eulerian adhesive stress closure that accounts for the effect of deformation history and the transition between the different flow regimes (fixed, expanded and fluidized bed states) in order to predict the hysteresis in the bed pressure drop at the macro-scale.

Some researchers have previously claimed that the standard two-fluid model, which does not account for adhesion between particles, can correctly predict the fluidization behavior of Geldart A particles if a sufficiently high resolution is used. For example, Wang et al. [73] demonstrated that fluidized bed expansion can be accurately predicted (compared to discrete particle simulations) when the cell size is of the order of three particle diameters and the time step is small. However, they only studied the bed expansion at superficial gas velocities well above the minimum fluidization velocity, at which the coordination number and hence the adhesive contribution may be negligible. Our two-fluid simulations employ a small time step and a cell size of two times the particle diameter, which complies with the recommendation of Wang et al. [73]. The results of these simulations reveal that no overshoot is generated during the transition from fixed to fluidized bed

without considering the effects of adhesion. Therefore, interparticle attractive forces may have a significant contribution to the hydrodynamic behavior observed in fluidized-bed experiments. Taking these adhesive interactions into account is critical for gaining a comprehensive understanding of the fluidization behavior of particles belonging to Geldart group A.

CRediT authorship contribution statement

Youssef Badran: Data curation, Investigation, Methodology, Resources, Validation, Visualization, Writing – original draft, Conceptualization. **Renaud Ansart:** Conceptualization, Funding acquisition, Methodology, Project administration, Resources, Software, Supervision, Validation, Writing – review & editing, Investigation. **Jamal Chaouki:** Conceptualization, Funding acquisition, Methodology, Project administration, Resources, Supervision, Validation, Writing – review & editing, Investigation. **Olivier Simonin:** Conceptualization, Methodology, Resources, Supervision, Validation, Writing – review & editing, Investigation.

Declaration of competing interest

The authors declare that they have no known competing financial interests or personal relationships that could have appeared to influence the work reported in this paper.

Data availability

Data will be made available on request.

References

[1] D. Kunii, O. Levenspiel, Fluidization Engineering, Butterworth-Heinemann, 1991, URL https://books.google.ca/books?id=ZVnb17qRz8QC.
[2] W.-c. Yang, Handbook of Fluidization and Fluid-Particle Systems, CRC Press, 2003, URL https://books.google.ca/books?id=lHTUphHZyogC.
[3] J.R. Grace, J. Chaouki, T. Pugsley, Fluidized bed reactor, Part. Technol. Appl. (2012) 199, http://dx.doi.org/10.1201/b11904.

[4] J. Shabanian, J. Chaouki, Effects of temperature, pressure, and interparticle forces on the hydrodynamics of a gas-solid fluidized bed, Chem. Eng. J. 313 (2017) 580–590, http://dx.doi.org/10.1016/j.cej.2016.12.061.

[5] P. Lettieri, D. Macrì, Effect of process conditions on fluidization, KONA Powder Part. J. 33 (2016) 86–108, http://dx.doi.org/10.14356/kona.2016017.

[6] J. Shabanian, R. Jafari, J. Chaouki, Fluidization of ultrafine powders, Int. Rev. Chem. Eng. 4 (1) (2012) 16–50.

[7] J. Ma, J.R. van Ommen, D. Liu, R.F. Mudde, X. Chen, S. Pan, C. Liang, Fluidization dynamics of cohesive Geldart B particles. Part II: Pressure fluctuation analysis, Chem. Eng. J. 368 (2019) 627–638, http://dx.doi.org/10.1016/j.cej.2019.02.187.

[8] G. Hendrickson, Electrostatics and gas phase fluidized bed polymerization reactor wall sheeting, Chem. Eng. Sci. 61 (4) (2006) 1041–1064, http://dx.doi.org/10.1016/j.ces.2005.07.029.

[9] P. Rajniak, C. Mancinelli, R. Chern, F. Stepanek, L. Farber, B. Hill, Experimental study of wet granulation in fluidized bed: Impact of the binder properties on the granule morphology, Int. J. Pharmaceut. 334 (1–2) (2007) 92–102, http://dx.doi.org/10.1016/j.ijpharm.2006.10.040.

[10] B.J. Skrifvars, M. Hupa, M. Hiltunen, Sintering of ash during fluidized bed combustion, Ind. Eng. Chem. Res. 31 (4) (1992) 1026–1030, URL https://pubs.acs.org/doi/pdf/10.1021/ie00004a008.

[11] P. Jiang, H. Bi, S.-C. Liang, L.-S. Fan, Hydrodynamic behavior of circulating fluidized bed with polymeric particles, AIChE J. 40 (2) (1994) 193–206, http://dx.doi.org/10.1002/aic.690400202.

[12] J. Shabanian, J. Chaouki, Hydrodynamics of a gas–solid fluidized bed with thermally induced interparticle forces, Chem. Eng. J. 259 (2015) 135–152, http://dx.doi.org/10.1016/j.cej.2014.07.117.

[13] E. Jaraiz, S. Kimura, O. Levenspiel, Vibrating beds of fine particles: estimation of interparticle forces from expansion and pressure drop experiments, Powder Technol. 72 (1) (1992) 23–30, http://dx.doi.org/10.1016/S0032-5910(92)85017-P.

[14] I. Soleimani, N. Elahipanah, J. Shabanian, J. Chaouki, In-situ quantification of the magnitude of interparticle forces and its temperature variation in a gas-solid fluidized bed, Chem. Eng. Sci. 232 (2021) 116349, http://dx.doi.org/10.1016/j.ces.2020.116349.

[15] S. Affleck, A. Thomas, A. Routh, N. Vriend, Novel protocol for quantifying powder cohesivity through fluidisation tests, Powder Technol. 415 (2023) 118147, http://dx.doi.org/10.1016/j.powtec.2022.118147.

[16] J. Visser, van der Waals and other cohesive forces affecting powder fluidization, Powder Technol. 58 (1) (1989) 1–10, http://dx.doi.org/10.1016/0032-5910(89)80001-4.

[17] J.N. Israelachvili, Intermolecular and Surface Forces, Academic Press, 2011, URL https://books.google.ca/books?id=vgyBJbtNOcoC.

[18] H.C. Hamaker, The London—van der Waals attraction between spherical particles, Physica 4 (10) (1937) 1058–1072, http://dx.doi.org/10.1016/S0031-8914(37)80203-7.

[19] F. London, The general theory of molecular forces, Trans. Faraday Soc. 33 (1937) 8b–26, http://dx.doi.org/10.1039/TF937330008B.

[20] C.Q. LaMarche, S. Leadley, P. Liu, K.M. Kellogg, C.M. Hrenya, Method of quantifying surface roughness for accurate adhesive force predictions, Chem. Eng. Sci. 158 (2017) 140–153, http://dx.doi.org/10.1016/j.ces.2016.09.024.

[21] Q. Li, V. Rudolph, W. Peukert, London-van der Waals adhesiveness of rough particles, Powder Technol. 161 (3) (2006) 248–255, http://dx.doi.org/10.1016/j.powtec.2005.10.012.

[22] H. Krupp, Particle adhesion theory and experiment, Advan. Colloid Interface Sci. 1 (1967) 111–239, http://dx.doi.org/10.1016/0001-8686(67)80004-6.

[23] B. Formisani, R. Girimonte, L. Mancuso, Analysis of the fluidization process of particle beds at high temperature, Chem. Eng. Sci. 53 (5) (1998) 951–961, http://dx.doi.org/10.1016/S0009-2509(97)00370-9.

[24] J. Shabanian, J. Chaouki, Fluidization characteristics of a bubbling gas–solid fluidized bed at high temperature in the presence of interparticle forces, Chem. Eng. J. 288 (2016) 344–358, http://dx.doi.org/10.1016/j.cej.2015.12.016.

[25] H. Piepers, E.J.E. Cottaar, A. Verkooijen, K. Rietema, Effects of pressure and type of gas on particle-particle interaction and the consequences for gas—solid fluidization behaviour, Powder Technol. 37 (1) (1984) 55–70, http://dx.doi.org/10.1016/0032-5910(84)80006-6.

[26] H.-Y. Xie, The role of interparticle forces in the fluidization of fine particles, Powder Technol. 94 (2) (1997) 99–108, http://dx.doi.org/10.1016/S0032-5910(97)03270-1.

[27] A. Srivastava, S. Sundaresan, Role of wall friction in fluidization and standpipe flow, Powder Technol. 124 (1–2) (2002) 45–54, http://dx.doi.org/10.1016/S0032-5910(01)00471-5.

[28] S. Mutsers, K. Rietema, The effect of interparticle forces on the expansion of a homogeneous gas-fluidized bed, Powder Technol. 18 (2) (1977) 239–248, http://dx.doi.org/10.1016/0032-5910(77)80014-4.

[29] S. Tsinontides, R. Jackson, The mechanics of gas fluidized beds with an interval of stable fluidization, J. Fluid Mech. 255 (1993) 237–274, http://dx.doi.org/10.1017/S0022112093002472.

[30] K. Rietema, H. Piepers, The effect of interparticle forces on the stability of gas-fluidized beds—I. Experimental evidence, Chem. Eng. Sci. 45 (6) (1990) 1627–1639, http://dx.doi.org/10.1016/0009-2509(90)80015-7.

[31] B. Liu, X. Zhang, L. Wang, H. Hong, Fluidization of non-spherical particles: Sphericity, Zingg factor and other fluidization parameters, Particuology 6 (2) (2008) 125–129, http://dx.doi.org/10.1016/j.cpart.2007.07.005.

[32] F. Vanni, B. Caussat, C. Ablitzer, M. Brothier, Effects of reducing the reactor diameter on the fluidization of a very dense powder, Powder Technol. 277 (2015) 268–274, http://dx.doi.org/10.1016/j.powtec.2015.03.010.

[33] S. Sánchez-Delgado, J.A. Almendros-Ibáñez, N. García-Hernando, D. Santana, On the minimum fluidization velocity in 2D fluidized beds, Powder Technol. 207 (1–3) (2011) 145–153, http://dx.doi.org/10.1016/j.powtec.2010.10.020.

[34] H. Matuttis, S. Luding, H. Herrmann, Discrete element simulations of dense packings and heaps made of spherical and non-spherical particles, Powder Technol. 109 (1–3) (2000) 278–292, http://dx.doi.org/10.1016/S0032-5910(99)00243-0.

[35] X.S. Wang, F. Rahman, M.J. Rhodes, Nanoparticle fluidization and Geldart's classification, Chem. Eng. Sci. 62 (13) (2007) 3455–3461, http://dx.doi.org/10.1016/j.ces.2007.02.051.

[36] J.W. Landry, G.S. Grest, L.E. Silbert, S.J. Plimpton, Confined granular packings: structure, stress, and forces, Phys. Rev. E 67 (4) (2003) 041303, http://dx.doi.org/10.1103/PhysRevE.67.041303.

[37] J.W. Landry, G.S. Grest, S.J. Plimpton, Discrete element simulations of stress distributions in silos: crossover from two to three dimensions, Powder Technol. 139 (3) (2004) 233–239, http://dx.doi.org/10.1016/j.powtec.2003.10.016.

[38] C.A. Ho, M. Sommerfeld, Modelling of micro-particle agglomeration in turbulent flows, Chem. Eng. Sci. 57 (15) (2002) 3073–3084, http://dx.doi.org/10.1016/S0009-2509(02)00172-0.

[39] S. Wang, H. Lu, Z. Shen, H. Liu, J. Bouillard, Prediction of flow behavior of micro-particles in risers in the presence of van der Waals forces, Chem. Eng. J. 132 (1–3) (2007) 137–149, http://dx.doi.org/10.1016/j.cej.2007.01.043.

[40] M. Zhang, K. Chu, F. Wei, A. Yu, A CFD–DEM study of the cluster behavior in riser and downer reactors, Powder Technol. 184 (2) (2008) 151–165, http://dx.doi.org/10.1016/j.powtec.2007.11.036.

[41] D. Gidaspow, L. Huilin, Equation of state and radial distribution functions of FCC particles in a CFB, AIChE J. 44 (2) (1998) 279–293, http://dx.doi.org/10.1002/aic.690440207.

[42] J.-F. Parmentier, Extension of the Euler/Euler Formalism for Numerical Simulations of Fluidized Beds of Geldart A Particles (Ph.D. thesis), Institut National Polytechnique de Toulouse, 2010, URL http://www.theses.fr/2010INPT0121/document. thesis directed by Olivier Simonin.

[43] J.T. Jenkins, D. Berzi, Dense inclined flows of inelastic spheres: tests of an extension of kinetic theory, Granul. Matter 12 (2) (2010) 151–158, http://dx.doi.org/10.1007/s10035-010-0169-8.

[44] S. Chialvo, J. Sun, S. Sundaresan, Bridging the rheology of granular flows in three regimes, Phys. Rev. E 85 (2) (2012) 021305, http://dx.doi.org/10.1103/PhysRevE.85.021305.

[45] S. Schneiderbauer, A. Aigner, S. Pirker, A comprehensive frictional-kinetic model for gas–particle flows: Analysis of fluidized and moving bed regimes, Chem. Eng. Sci. 80 (2012) 279–292, http://dx.doi.org/10.1016/j.ces.2012.06.041.

[46] P.N. Loezos, P. Costamagna, S. Sundaresan, The role of contact stresses and wall friction on fluidization, Chem. Eng. Sci. 57 (24) (2002) 5123–5141, http://dx.doi.org/10.1016/S0009-2509(02)00421-9.

[47] M. Ye, M.A. van der Hoef, J. Kuipers, The effects of particle and gas properties on the fluidization of Geldart A particles, Chem. Eng. Sci. 60 (16) (2005) 4567–4580, http://dx.doi.org/10.1016/j.ces.2005.03.017.

[48] M.W. Weber, C.M. Hrenya, Computational study of pressure-drop hysteresis in fluidized beds, Powder Technol. 177 (3) (2007) 170–184, http://dx.doi.org/10.1016/j.powtec.2007.01.016.

[49] M. Askarishahi, M.-S. Salehi, S. Radl, Capability of the TFM approach to predict fluidization of cohesive powders, Ind. Eng. Chem. Res. 61 (8) (2022) 3186–3205, http://dx.doi.org/10.1021/acs.iecr.1c04786.

[50] Y. Gu, A. Ozel, J. Kolehmainen, S. Sundaresan, Computationally generated constitutive models for particle phase rheology in gas-fluidized suspensions, J. Fluid Mech. 860 (2019) 318–349, http://dx.doi.org/10.1017/jfm.2018.856.

[51] Y. Wu, Q. Hou, A. Yu, Linking discrete particle simulation to continuum properties of the gas fluidization of cohesive particles, AIChE J. 66 (5) (2020) e16944, http://dx.doi.org/10.1002/aic.16944.

[52] H. Neau, M. Pigou, P. Fede, R. Ansart, C. Baudry, N. Mérigoux, J. Laviéville, Y. Fournier, N. Renon, O. Simonin, Massively parallel numerical simulation using up to 36,000 CPU cores of an industrial-scale polydispersed reactive pressurized fluidized bed with a mesh of one billion cells, Powder Technol. 366 (2020) 906–924, http://dx.doi.org/10.1016/j.powtec.2020.03.010.

[53] R. Ansart, P. García-Triñanes, B. Boissière, H. Benoit, J.P. Seville, O. Simonin, Dense gas-particle suspension upward flow used as heat transfer fluid in solar receiver: PEPT experiments and 3D numerical simulations, Powder Technol. 307 (2017) 25–36, http://dx.doi.org/10.1016/j.powtec.2016.11.006.

[54] B. Van Wachem, S. Sasic, Derivation, simulation and validation of a cohesive particle flow CFD model, AIChE J. 54 (1) (2008) 9–19, http://dx.doi.org/10.1002/aic.11335.

[55] P.C. Johnson, P. Nott, R. Jackson, Frictional–collisional equations of motion for participate flows and their application to chutes, J. Fluid Mech. 210 (1990) 501–535, http://dx.doi.org/10.1017/S0022112090001380.

[56] A. Srivastava, S. Sundaresan, Analysis of a frictional–kinetic model for gas–particle flow, Powder Technol. 129 (1–3) (2003) 72–85, http://dx.doi.org/10.1016/S0032-5910(02)00132-8.

[57] O. Simonin, Statistical and Continuum Modelling of Turbulent Reactive Particulate Flows, in: Lecture Series, vol. 6, 2000.

[58] X. He, G.D. Doolen, Thermodynamic foundations of kinetic theory and lattice Boltzmann models for multiphase flows, J. Stat. Phys. 107 (1) (2002) 309–328, http://dx.doi.org/10.1023/A:1014527108336.

[59] M. Elimelech, J. Gregory, X. Jia, R. Williams, Particle Deposition and Aggregation: Measurement, Modelling and Simulation, Elsevier Science, 2013, URL https://books.google.ca/books?id=R6g3BQAAQBAJ.

[60] R. Yang, R. Zou, A. Yu, Computer simulation of the packing of fine particles, Phys. Rev. E 62 (3) (2000) 3900, http://dx.doi.org/10.1103/PhysRevE.62.3900.

[61] C. Lun, S. Savage, The effects of an impact velocity dependent coefficient of restitution on stresses developed by sheared granular materials, Acta Mech. 63 (1) (1986) 15–44, http://dx.doi.org/10.1007/BF01182538.

[62] Q. Hou, Z. Zhou, A. Yu, Micromechanical modeling and analysis of different flow regimes in gas fluidization, Chem. Eng. Sci. 84 (2012) 449–468, http://dx.doi.org/10.1016/j.ces.2012.08.051.

[63] A. Gobin, H. Neau, O. Simonin, J.-R. Llinas, V. Reiling, J.-L. Sélo, Fluid dynamic numerical simulation of a gas phase polymerization reactor, Int. J. Numer. Methods Fluids 43 (10–11) (2003) 1199–1220, http://dx.doi.org/10.1002/fld.542.

[64] C. Wen, Y. Yu, Mechanics of fluidization, in: Chem. Eng. Prog. Symp. Ser., Vol. 62, 1966, pp. 100–111, URL https://cir.nii.ac.jp/crid/1572261550060180736.

[65] S. Ergun, Fluid flow through packed columns, Chem. Eng. Prog. 48 (2) (1952) 89–94, URL https://cir.nii.ac.jp/crid/1572543025220678016.

[66] O. Simonin, E. Deutsch, J. Minier, Eulerian prediction of the fluid/particle correlated motion in turbulent two-phase flows, Appl. Sci. Res. 51 (1993) 275–283, http://dx.doi.org/10.1007/BF01082549.

[67] P. Fevrier, O. Simonin, Constitutive relations for fluid-particle velocity correlations in gas-solid turbulent flows, in: Third International Conference on Multiphase Flows, ICMF, Vol. 98, 1998, pp. 8–12.

[68] F. Fotovat, R. Ansart, M. Hemati, O. Simonin, J. Chaouki, Sand-assisted fluidization of large cylindrical and spherical biomass particles: Experiments and simulation, Chem. Eng. Sci. 126 (2015) 543–559, http://dx.doi.org/10.1016/j.ces.2014.12.022.

[69] Y. Badran, R. Ansart, J. Chaouki, O. Simonin, Effect of Van der Waals force on fluidization of fine particles, in: 13th International Conference on Fluidized Bed Technology, CFB-13, Vancouver, Canada, 2021, pp. 124–129.

[70] C. Goldenberg, A.P. Atman, P. Claudin, G. Combe, I. Goldhirsch, Scale separation in granular packings: stress plateaus and fluctuations, Phys. Rev. Lett. 96 (16) (2006) 168001, http://dx.doi.org/10.1103/PhysRevLett.96.168001.

[71] J. Zhang, T. Majmudar, A. Tordesillas, R. Behringer, Statistical properties of a 2D granular material subjected to cyclic shear, Granul. Matter 12 (2010) 159–172, http://dx.doi.org/10.1007/s10035-010-0170-2.

[72] S. Luding, Anisotropy in cohesive, frictional granular media, J. Phys.: Condens. Matter 17 (24) (2005) S2623, http://dx.doi.org/10.1088/0953-8984/17/24/017.

[73] J. Wang, M.A. van der Hoef, J. Kuipers, Why the two-fluid model fails to predict the bed expansion characteristics of Geldart A particles in gas-fluidized beds: a tentative answer, Chem. Eng. Sci. 64 (3) (2009) 622–625, http://dx.doi.org/10.1016/j.ces.2008.09.028.